JOURNAL OF MATERIALS SCIENCE 25 (1990) 1568–1584

# Thermodynamically reversible and irreversible control on morphology of multiphase systems

## Part 1 *Rayleigh–Brillouin laser light scattering study on miscibilities and phase diagrams of rubber-modified epoxies*

HENRY S.-Y. HSICH
*Lord Corporation, Thomas Lord Research Center, 405 Gregson Drive, Cary, North Carolina 27512, USA*

Morphology and properties of polymer alloys can be controlled by thermodynamically reversible (structure frozen-in) or irreversible (structure locked-in) processes by simultaneously manipulating miscibility, mechanisms of phase separation, glass transitions, and cure kinetics of polymer systems. A new method of using Rayleigh–Brillouin laser light scattering experiments for constructing phase diagrams consisting of the binodal and spinodal curves has been developed. The Brillouin spectra can also be used to study cure kinetics of thermosetting materials. The miscibility of an epoxy/carboxyl-terminated butadiene acrylonitrile copolymer (CTBN) rubber system has been studied by this new method. It was found that this system has an upper consolute temperature. An increase in the acrylonitrile content of the CTBN rubber improves the miscibility and depresses the consolute temperature of this polymer system. The miscibility gap (the consolute temperature) can be shifted up and down by the presence of different curing agents. The morphology of this epoxy/CTBN system can be controlled by simultaneously manipulating the kinetic processes of phase separation and curing reactions.

## 1. Introduction

Multicomponent polymer systems such as polymer blends or polymer alloys have recently attracted considerable interest as a new and important challenge for researchers. The ultimate goal of using multicomponent polymer systems is to achieve commercially viable products through either unique properties or low cost.

Polymer blends and polymer alloys are often used synonymously; however, thermodynamically speaking, there is a distinction between these two terms. Polymer alloys are conditionally miscible thermodynamically. This means that the components of the alloy are homogeneous (single phase) under at least one specific set of thermodynamic conditions. Alloys as such provide the opportunity to change morphology and properties through variations in thermal history. Polymer blends, however, do not form single-phase systems under any thermodynamic conditions. Their properties are largely dependent on mechanical dispersion and are usually tied to the arithmetic average of the values, at most, of the components. Polymer alloys can be synergistic polymer systems. As such, their properties can exceed a simple arithmetic averaging value (additive rule) of multicomponent systems.

Compatibilizers can either enhance the miscibility (single-phase thermodynamically) of polymer alloys or improve the compatibility (good dispersion) of polymer blends. By adding the proper compatibilizer, the miscibility zone of the polymer alloy can be expanded; in some cases, an immiscible polymer mixture (polymer blend) can become a conditionally miscible mixture thermodynamically of a polymer alloy. While compatibilizers rarely render polymer blends miscible, the compatibilizer will (1) reduce the interfacial energy between the phases (components), (2) permit a finer dispersion during mixing, (3) provide a measure of stability against gross segregation, and (4) result in improved interfacial adhesion [1].

Only polymer alloys can give superior properties far beyond the additive rule. For this reason, this research programme concentrates on polymer alloys instead of polymer blends. Enhancing the miscibility of polymer mixtures by compatibilizing agents is one of the most commercially attractive methods for making polymer alloys [1]. Graft or block copolymers (AB) can be used to enhance the miscibility of polymer mixtures A and B. Varying the molecular weight of each segment in the block copolymer provides a means to control the miscibility gap (phase-separation temperature) of the polymer system. This, in turn, is a method to control morphology and properties. The miscibility zone will be expanded when the molecular weights of the corresponding segments molecular weights in the block copolymer are increased to larger than those of the homopolymers.

Mixing polymers having high molecular weights



0022–2461/90 $03.00 + .12 

leads to a very small increase in entropy. Therefore, combinations of polymer pairs which give a decrease in enthalpy must be found in order to obtain miscible polymer systems. One can also achieve miscibility enhancement by other methods. Modifying the polymers to induce hydrogen bonding [2–4], donor–acceptor interactions [5, 6], dipole–dipole interactions [7, 8], anion–cation interactions [9, 10], and ion–dipole interactions [11, 12] between the two polymers are examples.

There are several important factors in controlling the mechanical strength of materials. These are bonding energy, elastic energy, tearing energy and morphology. Proper control of morphological structure can drastically improve the mechanical strength of materials. This concept has been demonstrated previously [13]. The ideal mechanical strength of a material should be close to the modulus of the material. However, for most materials, particularly glasses, the mechanical strength is at least three orders of magnitude lower than the modulus. Hsich demonstrated that the mechanical strength of a glass could be increased more than two orders of magnitude by controlling the morphology of that glass. This was accomplished by eliminating stress concentrations, microvoids and surface flaws [13].

The purpose of adding elastomers to thermoset or thermoplastic matrices is to modify the fracture behaviour of these systems. It is believed that the elastomeric particles act as energy absorbers or crack stoppers in such systems [16–18]. The effectiveness in improving the fracture behaviour of rubber-modified systems depends on the ability to control the morphology in these systems. For example, particle sizes or domain structures of the rubber-rich phase and the degree of phase mixing between the two-phase boundary are primary factors for improving mechanical strength and adhesion properties of multicomponent systems. In order to manipulate the morphology, an understanding of the miscibility and phase separation in multicomponent systems must be obtained.

In this report we will discuss the miscibility, and the thermodynamic and kinetic processes of phase separation. The control of morphology by the kinetic processes of phase separation either via nucleation and growth (NG) or spinodal decomposition (SD) will also be discussed. A new method of constructing phase diagrams consisting of both binodal and spinodal curves via Raleigh–Brillouin laser light scattering will be introduced. Further, the concept of controlling morphology by simultaneously manipulating the kinetic processes of phase separation and curing reactions will be discussed.

The applications for polymer alloys as engineering materials, adhesives, telecommunication and electronic materials, membranes, and damping materials are unlimited. In this research programme, we began with rubber-modified thermosets. Rubber-modified epoxies have been widely used as high-performance engineering materials, structural adhesives, electronic packaging materials and information storage media.

## 2. Background

### 2.1. Miscibility and phase separation of multicomponent systems

#### *2.1.1. Miscibility and phase diagrams*

Critical solution phenomena and miscibility in multicomponent systems were discussed extensively by Prigogine and Defay [19]. Recently, Krause [20] and Kwei and Wang [21] also gave a review on polymer systems. Phase diagrams of multiphase polymers can be a system with (a) an upper critical solution temperature (UCST), (b) a lower critical solution temperature (LCST), (c) an LCST above a UCST, (d) a closed two-phase region, and (e) a bell-shaped two-phase region, as shown in Fig. 1. For a system containing a simple miscibility gap of high consolute temperature (UCST system), at a constant temperature above the consolute temperature, $T_c$ (sometimes called critical temperature), the Helmholz free energy, $G$, must curve upward everywhere. As the temperature drops below $T_c$, the Helmholz free energy at a given temperature, $T_0$, will vary with composition, $c$, as depicted by the top curve of Fig. 2. The points of common tangency to this curve ($f$ and $g$, Fig. 2) define the composition of two co-existing phases at $T_0$ (binodal points). If the composition lies between the compositions $a$ and $b$, the lowest free energy is a two-phase mixture with one phase having composition $a$ and the other $b$.

In addition, there are two inflexion points at which $(\partial^2 G/\partial^2 c)$ vanishes, these two points occur at $d$ and $e$ and are called the spinodal points for the temperature $T_0$, lying somewhere between $a$ and $b$. Between these two spinodal points, $(\partial^2 G/\partial^2 c)$ is negative, and the mixture is said to be in an unstable state, because any infinitesimal composition fluctuations will cause a decrease in the free energy and hence phase separation. The metastable region exists between the spinodal and the binodal curve (phase boundary). If the single phase is cooled from above the phase boundary into this region, it would be metastable and would only decompose into the two phases if the second phase can nucleate. Any attempt by the system to separate into regions differing only slightly in composition will raise the system free energy. If, however, the single phase is brought within the unstable region (between points $d$ and $e$) the system can continuously lower its free energy by continuous compositional change until it reaches a two-phase state at $a$ and $b$.

#### *2.1.2. Kinetics of phase separation and morphology*

The mechanism of phase separation in the two regions, metastable and unstable, are radically different. In the unstable region, the mixture is unstable to infinitesimal fluctuations. There is no thermodynamic barrier to phase transformation, and thus, separation should occur by a continuous and spontaneous process. Because the mixture is initially uniform in composition, this spontaneous process must occur by a diffusional flux against the concentration gradient, that is, by uphill diffusion with a negative diffusion coefficient. There is no sharp interface boundary between the phases in the initial stage of this type of

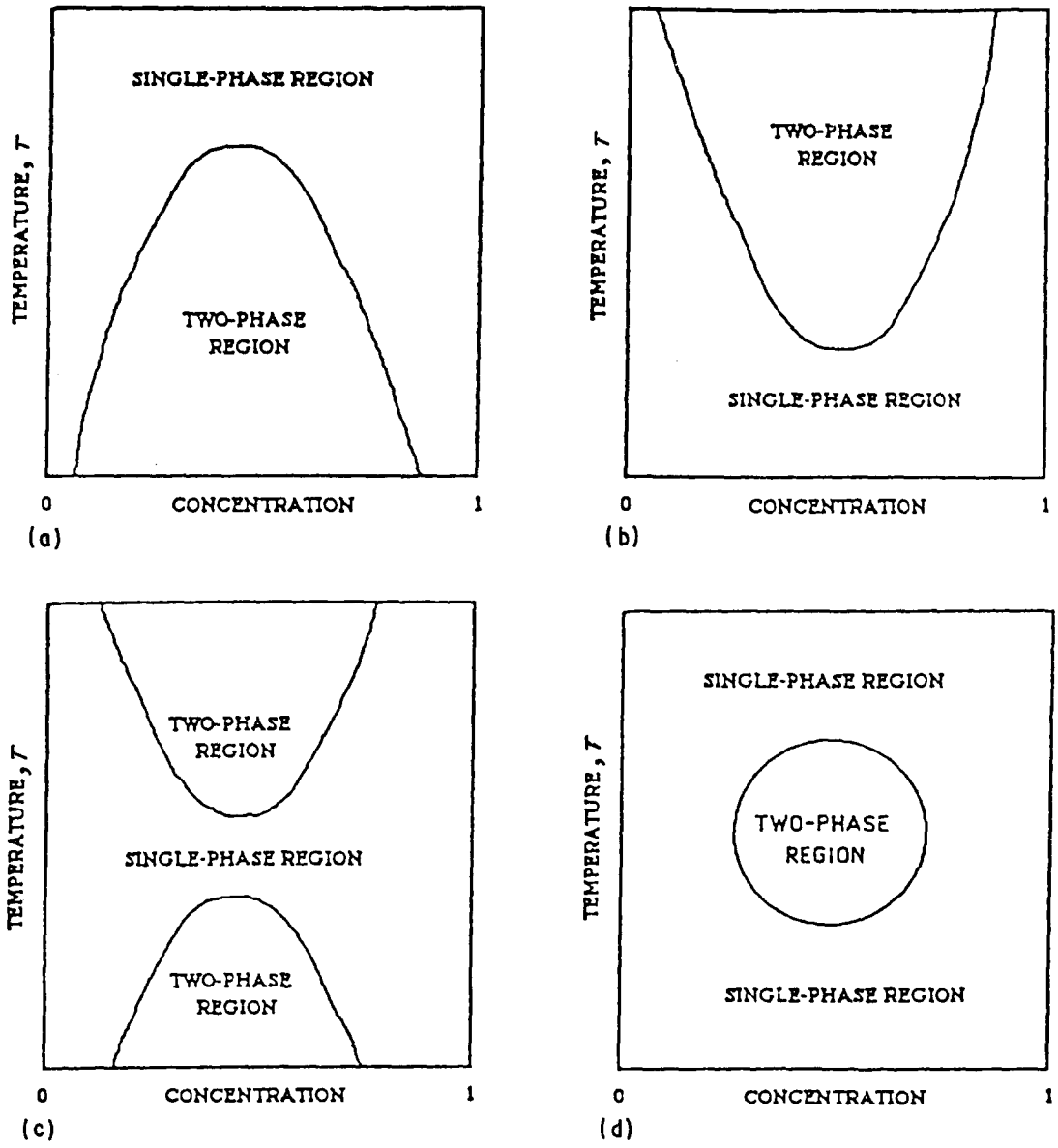


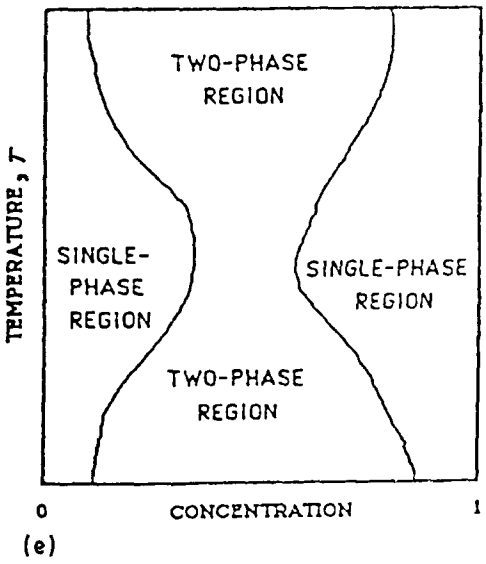


*Figure 1* (a) to (e) Phase diagrams of polymer systems.

phase separation. This process is called spinodal decomposition (SD).

On the other hand, in the metastable region, because the mixture is stable to all infinitesimal composition fluctuations, a finite fluctuation is required for a phase transformation. The new phase starts from small nuclei which then proceed to grow and extend. The molecules that feed the new phase follow ordinary transport phenomena by downhill diffusion with a positive diffusion coefficient. This process is called nucleation and growth (NG).

*2.1.2.1. Nucleation and growth.* The theory of phase transition $\alpha$ to $\delta$ has been discussed by Turnbull [22]. In general, this transition does not occur homogeneously. Rather, small domains of phase $\delta$ first become distinct at various points separated by many molecular spacings. These domains then propagate at the expense of $\alpha$. Thus, the transformation $\alpha$ to $\delta$ takes place only at the $\alpha$ and $\delta$ interfaces. This mode of reaction is known as nucleation and growth, the birth of domains being called nucleation. However, if the compositions making up $\alpha$ and $\delta$ are markedly different (as happens in phase separation of multicomponent systems), the growth of $\delta$ may be governed by the diffusion of its components in $\alpha$ rather than by processes at the $\alpha$–$\delta$ interface. The total rate of a phase change is determined by two constants: the rate of nucleation, $J$, of $\delta$ domains and their rate of growth, $u$, after nucleation.

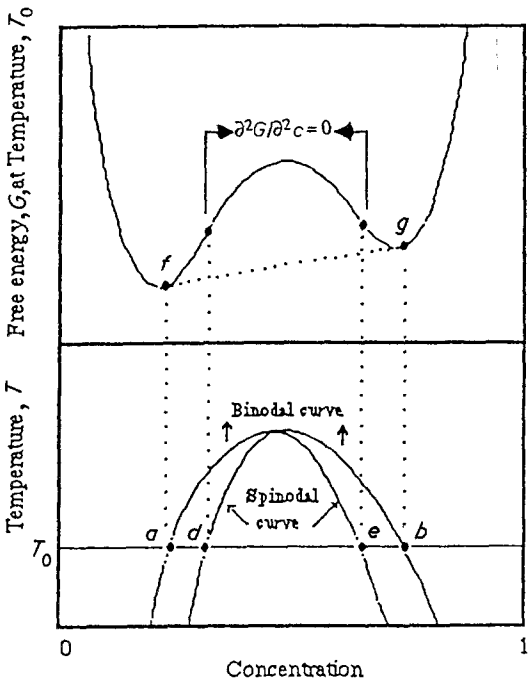


*Figure 2* Phase diagram of binodal and spinodal curve.

The impedance to the formation of a new phase is associated with the extra surface energy of small clusters that make their formation difficult. Such clusters, if small, are called germs and, if somewhat large and recognizable as precursors to the new phase, are called nuclei. The smaller cluster (germ) will, on average, completely dissociate after a time, because its standard free energy increases with the addition of molecules. However, a larger cluster (nucleus) will continue to grow, on average, and become a domain of the new phase, because its standard free energy is continuously decreased thereby. Thus, to become a nucleus, a cluster must acquire (by growing to a critical size) a critical standard free energy, $\Delta G^*$ (thermodynamic barrier), in excess of that of single molecules. The nucleation frequency, $J$, per unit volume is proportional to the following factors

$$J \propto N \exp(-\Delta G^*/k_B T) \quad (1)$$

where $N$ is the number of single molecules of the new phase, $k_B$ is the Boltzmann constant, and $T$ is the absolute temperature.

The volume, $v$, of a $\delta$ domain which grows at a constant linear rate is given by

$$v = g u^3 (t - \tau)^3 \quad (2)$$

where $g$ is a shape factor, $t$ is the total transformation time, and $\tau$ is the time since the beginning of transformation at which the $\delta$ domain nucleated.

Then the total transformed volume $x$ can be expressed as follows:

$$x = 1 - \exp\left[-\int_0^t vJ \, d\tau\right] \quad (3)$$

where the volume of the system is assumed to be unity for all $x$ values. The kinetic data can often be described approximately by the equation

$$x = 1 - \exp[-bt^m] \quad (4)$$

$b$ and $m$ are the parameters of the multiphase system. One should keep in mind that the morphology developed by the mechanism of NG has a sharp boundary between interfaces. The morphology of the second phase is an isolated droplet structure during the initial stage of NG.

In the metastable region, two basic stages of phase development may be distinguished. The first is the nucleation and growth stage during which concentration fluctuations produce nuclei of the new phase which grow from the super-saturated matrix. The second stage is the coalescence process (Ostwald ripening stage). During this coarsening stage, the total surface of the dispersed phase is reduced. Fluctuation effects play a negligible part in this stage. In this stage, the average diameter, $D$, of the particles is seen to obey a kinetic law of the Lifshitz–Slyozov–Wagner asymptotic law [23–25]. The equation for the asymptotic law can be expressed as

$$D^3 - D_0^3 = \gamma(t - t_0) \quad (5)$$

where $D_0$ is the diameter of the particle corresponding to the time $t_0$ from which Equation 5 starts to be obeyed, and $\gamma$ is the rate constant.

*2.1.2.2. Spinodal decomposition.* Spinodal decomposition is one of the few phase transformations in which the kinetic theory has been well studied [26–34]. The reason for this is that the entire decomposition process can be treated as a purely diffusional problem and, further, many of the characteristics of decomposition, especially morphology, can be described by an approximate solution to the diffusion equation. Since Cahn [29] and Cahn and Charles [30] have demonstrated that glasses may undergo spinodal decomposition (SD), there has been widespread tendency to assume that the kinetic mechanisms for all those demixing processes which lead to textures displaying some degree of connectivity must be spinodal decomposition. This extreme view, however, cannot be justified, as other mechanisms, for example (as has been suggested by Haller [35]), nucleation and growth followed by coalescence, may also lead to similar formations. Conclusions reached from a mere inspection of an electron micrograph are certainly insufficient and may be grossly misleading. Only a detailed analysis of thermodynamics in the miscibility gap (or phase diagram) and the initial kinetic process can show whether, in a given case, we are indeed dealing with spinodal decomposition.

According to the theory of spinodal decomposition [26, 29], in an inhomogeneous solution the composition everywhere differs only slightly from the average composition. The free energy is given by

$$G = \int [g(c) + \kappa(\Delta c)^2] \, dV \quad (6)$$

Here $g(c)$ is the free energy density of the homogeneous material having composition $c$, $\kappa(\Delta c)^2$ is the additional free energy density if the material is in a gradient in composition, and $\kappa$ is the gradient energy coefficient and is positive. If $g(c)$ is expanded about

the average composition, $c_0$, then

$$g(c) = g(c_0) + (c - c_0)(\partial g/\partial c) + 1/2\,(c - c_0)^2(\partial^2 g/\partial^2 c) + \ldots \quad (7)$$

The free energy difference between the initially homogeneous solution and the inhomogeneous solution is given as

$$\Delta G = \int [1/2\,(\partial^2 g/\partial^2 c)(c - c_0)^2 + \kappa(\Delta c)^2]\,dV \quad (8)$$

The diffusion equation which takes into account the gradient energy terms encountered in spinodal decomposition can be written as [29]

$$\partial c/\partial t = M[(\partial^2 g/\partial^2 c)\nabla^2 c - 2\kappa\nabla^4 c] + \text{nonlinear terms} \quad (9)$$

where $M$ is the molecular mobility. For the initial stages of spinodal decomposition it is valid to ignore the nonlinear terms. Then the local concentration (or composition) $c(\mathbf{r}, t)$ of the solution at time $t$ at a point in space defined by the position vector $\boldsymbol{r}$ may be analysed in terms of its Fourier components by the expression:

$$c(\boldsymbol{r}, t) - c_0 = \sum \exp[R(\beta)t]\,[A(\beta)\cos(\boldsymbol{\beta}\cdot\boldsymbol{r}) + B(\beta)\sin(\boldsymbol{\beta}\cdot\boldsymbol{r})] \quad (10)$$

The summation $\Sigma$ is over all wave vector $\beta$. $A$ and $B$ are to be evaluated at $t = 0$ by Fourier analysing the fluctuations in the initial solution. The amplification factor $R(\beta)$ is given by

$$R(\beta) = -M(\partial^2 g/\partial^2 c)\beta^2 - 2M\kappa\beta^4 \quad (11)$$

The solution of Equations 10 and 11 tells us that any sinusoidal component present initially in the composition profile of a specimen will grow or shrink exponentially according to whether $R(\beta)$, the amplification factor, is positive or negative. Outside the spinodal region, $(\partial^2 G/\partial^2 c) > 0$; consequently $R(\beta)$ is negative for all values of $\beta$ and any existing fluctuation will diminish with time. Therefore, the system should homogenize. For this reason, a continuous and spontaneous process of concentration decomposition resulting in the formation of a periodic or quasi-periodic texture can only occur in the unstable region where $(\partial^2 G/\partial^2 c)$ is negative.

In the spinodal region, the critical value wave number, $\beta_c$, is given by the value

$$\beta_c^2 = -1/2\kappa\,(\partial^2 g/\partial^2 c) \quad (12)$$

$\beta_c$ corresponds exactly to a wavelength where all the contributions to the free energy cancel each other out, and forms the boundary between positive and negative $R(\beta)$. A wavelength with $\beta < \beta_c$ will grow and $\beta > \beta_c$ will shrink.

The interdiffusion coefficient $D$ is defined by the expression

$$D = M(\partial^2 g/\partial^2 c) \quad (13)$$

Then Equation 11 can be rewritten as

$$R(\beta) = -D\beta^2(1 - \beta^2/\beta_c^2) \quad (14)$$

$M$ is always positive, $D$ is negative within the spinodal, which corresponds to an *uphill* diffusion. From Equation 14 it is seen that the maximum of $R(\beta)$ occurs for a wavenumber $\beta_m = \beta_c/2^{1/2}$. The spatial components of wavelength $\lambda_m = 2\pi/\beta_m$ is called the spinodal wavelength of the system. Because $R(\beta)$ has a steep maximum and because it occurs in an exponential in Equation 10, it is convenient to ignore the growth of all wavelengths but those near the fastest growing ones. This principle of selective amplification is a good first approximation. Then Equation 10 can be approximated as

$$c(\boldsymbol{r}, t) - c_0 \approx A(\beta_m)\exp[R(\beta_m)t]\cos(\boldsymbol{\beta}_m\cdot\boldsymbol{r}) \quad (15)$$

where

$$R(\beta_m) = -1/2\beta_m^2 D \quad (16)$$

By setting $R(\beta_m) = 1/t$, Equation 16 is but a variant of the well-known expression for the square of diffusion distance

$$\lambda_m^2 = 2(2\pi)^2|D|\,t \quad (17)$$

Now the time constant for spinodal decomposition can be estimated by setting $\lambda_m = 10\,\text{nm}$ (size of domain structure)

$$t \approx 10^{-13}/|D| \quad (18)$$

Thus in fluid liquids with interdiffusion coefficient $|D| \approx 10^{-6}\,\text{cm}^2\,\text{sec}^{-1}$, the time constant is less than microseconds. There would be no hope of cooling (or heating) a liquid fast enough to suppress the sinodal reaction even one degree below (or above) the spinodal. Because $|D|$ for a solid near the melting point is typically $10^{-9}\,\text{cm}^2\,\text{sec}^{-1}$, the time constant is still milliseconds. Only in solids in which the spinodal is well below the melting point is there any hope of finding a time scale long enough to suppress the reaction for studying it isothermally. However, one can easily study the mechanisms of spinodal decomposition in polymer systems by increasing molecular weights of the polymers or by introducing crosslinking reactions for reducing the interdiffusion coefficient.

It should be mentioned here, that the unique morphology created by the initial stage of its spinodal decomposition consists of an interface between two coexisting phases which is diffuse and its thickness increases with decreasing $\Delta T$ ($\Delta T = |T - T_s|$) and becomes infinite at the spinodal temperature, $T_s$. $T_s$ is the temperature at the spinodal curve. The periodic domain structure, $\lambda_m$, varies with the heat-treatment temperature, $T$, and is described by

$$1/\lambda_m^2 = q|T - T_s| \quad (19)$$

where $q$ is a constant depending on the system.

In the second stage of the spinodal decomposition, the domain structure becomes large and the rate of growth of the composition fluctuation amplitude is slowed down. This period corresponds to a coarsening of the texture. This process is an Ostwald ripening process where differences in solute concentration due to various particle sizes set up concentration gradients which tend to resorb smaller particles and make the large ones grow at their expense. We have discussed this type of coarsening mechanism in the section of nucleation and growth.

## 2.2. Rayleigh–Brillouin laser light scattering study on the miscibility of multiphase systems

In the above discussions, it was mentioned that there are two different mechanisms (nucleation and growth, and spinodal decomposition) controlling phase separation. These two mechanisms will give different kinetic rates and different morphological structures. Therefore, understanding the miscibility of phase diagrams of polymer systems is of monumental importance for manipulating the morphology and properties of materials. In the following, we will introduce the concept of using Rayleigh–Brillouin laser light scattering for constructing the binodal and spinodal curves that make up the phase diagrams of multiphase systems. Rayleigh–Brillouin scattering has been used by Hsich *et al.* [36] for studying the phase separation of multiphase systems. Hsich [37] further discussed the utility of Rayleigh–Brillouin scattering experiments as an effective method for studying chemical relaxation, such as hydration reactions, dissolution of solid state reactions, or cure reactions.

From Einstein's classical theory of light scattering [38], the scattering intensity $I_T$ is proportional to the density fluctuation, and it can be expressed as

$$I_T(\theta) = I_0(k_0^4/32\pi^2R_0^2)\,(1 + \cos^2\theta)\,\langle(\Delta\varepsilon)^2\rangle \quad (20)$$

For a two-component system, according to the thermodynamic fluctuation theory [39], $\langle(\Delta\varepsilon)^2\rangle$ can be expressed as

$$\langle(\Delta\varepsilon)^2\rangle = (\partial\varepsilon/\partial\varrho)^2_{T,c}\,\langle(\Delta\varrho)^2\rangle + (\partial\varepsilon/\partial T)^2_{\varrho,c}\,\langle(\Delta T)^2\rangle + (\partial\varepsilon/\partial c)^2_{\varrho,T}\,\langle(\Delta c)^2\rangle \quad (21)$$

where $I_0$ is the intensity of the incident beam, $k_0$ is the wave vector associated with this beam, $R_0$ is the distance from the scattering volume, $V$, to the detector, $\theta$ is the angle between the incident and scattered wave. $\varepsilon$, $\varrho$ and $x$ are dielectric constant, density and concentration, respectively. $\langle(\Delta\varepsilon)^2\rangle$, $\langle(\Delta\varrho)^2\rangle$, and $\langle(\Delta c)^2\rangle$ are the mean square fluctuations of the dielectric constant, density and concentration, respectively.

For most liquids, the second term in Equation 21 is small compared with the other terms. Therefore, according to Hsich *et al.* [36], Equation 21 can be expressed as

$$\langle(\Delta\varepsilon)^2\rangle = (\varrho\partial\varepsilon/\partial\varrho)^2_{T,c}\,(k_BT/V)\,\{\kappa_S(\omega_B) + [\kappa_S(0) - \kappa_S(\omega_B)] + [\kappa_T(0) - \kappa_S(0)]\} + (\partial\varepsilon/\partial c)^2_{\varrho,T}\,(k_BT)/(\partial^2G/\partial^2c)_{P,T} \quad (22)$$

where $k_B$ is Boltzmann's constant, $T$ is the absolute temperature, $\kappa_S$ and $\kappa_T$ are the adiabatic and isothermal compressibility, respectively, and $G$ is the Gibbs free energy. In dispersion liquids, the dynamic compressibility $\kappa_S(\omega_B)$ will be different from the equilibrium value $\kappa_S(0)$.

There are four terms in Equation 22. The first two terms are due to pressure fluctuations. The first term is proportional to $\kappa_S(\omega_B)$ which propagates with an acoustic frequency, $\omega_B$, and is the source of the Brillouin doublet. The second term is proportional to $[\kappa_S(0) - \kappa_S(\omega_B)]$ which will not propagate when the structural relaxation time of liquids is much larger than the inverse of the acoustic frequency, $\omega_B$ (such as near the glass transition or in the glassy state). This portion of the spectrum will be relaxed to the central Rayleigh component, and it is called the Mountain-line. The third term presents local entropy fluctuations which do not propagate and are the source of the unshifted central Rayleigh component. The last term is due to composition fluctuations which also do not propagate and are another source of the Rayleigh component. We can write the scattering intensity of the Brillouin doublet as

$$2I_B = I_0(k_0^4/32\pi^2R_0^2)\,(1 + \cos^2\theta)\,(\varrho\partial\varepsilon/\partial\varrho)^2_{T,c} \times (k_BT/V)\kappa_S(\omega_B) \quad (23)$$

and Rayleigh component as

$$I_R = I_0(k_0^4/32\pi^2R_0^2)\,(1 + \cos^2\theta)\,\{(\varrho\partial\varepsilon/\partial\varrho)^2_{T,c}(k_BT/V) \times [(\kappa_T(0) - \kappa_S(0)) + (\kappa_S(0) - \kappa_S(\omega_B))] + (\partial\varepsilon/\partial c)^2_{\varrho,T}\,(k_BT)/(\partial^2G/\partial^2c)_{P,T}\} \quad (24)$$

The ratio of the intensity of the Rayleigh central component, $I_R$, to that of the Brillouin doublet, $2I_B$, is called the Landau–Placzek ratio which can be written as

$$R_{LP} = I_R/2I_B \quad (25)$$

According to the classical theory of free energy expansion [40], the excess free energy of the system can be rewritten from Equation 7 as a power series expansion in powers of $(c - c_0)$, the difference in concentration from the critical concentration, $c_0$

$$G - G_0 = a_1\,(c - c_0) + (a_2/2)(T - T_c)(c - c_0)^2 + (a_4/12)(c - c_0)^4 + \ldots \quad (26)$$

where $a_i$ is the coefficient of the free energy expansion, and $T_c$ is the critical temperature of the multiphase system.

By using Equation 23, the Rayleigh intensity contributed from the composition fluctuations can be expressed as

$$I_c = I_0(k_0^4/32\pi^2R_0^2)\,(1 + \cos^2\theta)\,(\partial\varepsilon/\partial c)^2_{\varrho,T} \times (k_BT)/[a_2(T - T_S)] \quad (27)$$

where $T_S$ is the so-called spinodal temperature

$$T_S = T_c - (a_2/a_4)(c - c_0)^2 \quad (28)$$

and terms of a higher than second order have been ignored.

Kadanoff *et al.* [40] have given a general review of critical fluctuation phenomena in which they point out that the classical theory can only be valid when the range of correlations for fluctuations in the critical ordering parameter is relatively small. From this they show that any attempt to use classical theory must be restricted to the temperature range for which

$$(T - T_c)/T_c \gg (1/32\pi^2)\,[2k_B/3a_2(a_2/a_4)T_c\Lambda_D^3]^2 \quad (29)$$

where $\Lambda_D$ is the Debye correlation length.

According to Ornstein and Zernike [41, 42], with the temperature close to the critical point, the resultants

of density fluctuations or composition fluctuations can have an effect on the state of the medium at distances that are much greater than the radius of molecular interaction under normal conditions. Therefore, the Debye correlation length becomes very large. Consequently, the scattering intensity never has the chance to reach divergence as predicted by Equation 27. Nevertheless, one can construct the spinodal curve of a phase diagram for a multiphase system by calculating the Landau–Placzek ratio as a function of the temperature in doing a super-critical (above the upper consolute temperature) study of the Rayleigh–Brillouin scattering. From Equations 23 to 25 and 27, the Landau–Placzek ratio can be written as a function of $(T - T_S)$ [36]:

$$R_{LP} = \alpha^2 T v(\omega_B)^2 / C_p + [v(\omega_B)^2 - v_0^2]/v_0^2 + (\partial\varepsilon/\partial c)_{\varrho,T}^2 V/\{(\varrho\partial\varepsilon/\partial\varrho)_{T,c}^2 [a_2(T - T_S)]\} \quad (30)$$

where $\alpha$ is the thermal expansion, $C_p$ is the heat capacitance at a constant pressure, and $v(\omega_B)$ and $v_0$ are sound speed at the Brillouin frequency and zero frequency, respectively.

## 3. Thermodynamically reversible and irreversible control of morphology–structure frozen-in and structure locked-in

As we have mentioned, the phase separation process, either by nucleation and growth or by spinodal decomposition, is a diffusion control process. Therefore, to be able to control morphology as discussed by Cahn [31], the miscibility gap (binodal and spinodal curves) must be at or below the glass transition temperature, $T_g$, or liquidus temperature. However, Hsich [43] pointed out that in thermosetting or elastomeric systems, the morphological structure can be manipulated via cure kinetics and phase separation processes even though the miscibility gaps of the polymer systems are far above the $T_g$ of the uncured polymers. During cure, the changes of molecular weight and network structure not only cause the miscibility gap to shift but also increase $T_g$ of the polymers. For these reasons, if cure kinetics and phase separation processes are properly manipulated, the morphology of polymers can be controlled.

There are two different approaches, depending on whether the material is cross-linked, in controlling the morphology of multiphase systems. For a non-cross-linked polymer system, the morphology of a material is controlled by a thermodynamically reversible process (*structure frozen-in*) during the cooling stage to reach its glassy state. In this case, to control the morphology, one must choose a system in which phase separation is slow compared with the time it takes to change the temperature of the samples. This type of polymer system must have a miscibility gap (phase separation temperature) near $T_g$. The speed of phase separation depends on the diffusion coefficient which is related to the relaxation time [44] of the glassy materials. To control effectively the morphology of these polymer systems, one must apply the miscibility gap and the structural relaxation phenomena of the polymer systems. Aspects of nonequilibrium thermodynamics and structural relaxation of the glassy state have been discussed by Davies and Jones [45], Staverman [46], and Hsich [47–49].

To control morphology of a cross-linkable material, such as epoxies or thermoset elastomeric materials, one can control the morphology of the material by simultaneously manipulating the kinetic processes of the cure reactions and phase separation (thermodynamically irreversible, *structure locked-in*). In doing so, the cure kinetics of the polymer systems is of vital importance. Recently, Hsich [50] and Hsich *et al.* [51–53] developed a kinetic model of cure which is able to predict the change of rheological and mechanical properties during the entire cure cycle. By incorporating the cure model along with the kinetics of phase separation, one can control the morphology of these multiphase systems.

## 4. Phase diagram and morphology of epoxy–CTBN rubber

Drake and McCarthy [54] found that the incorporation of low levels of a liquid carboxyl-terminated butadiene acrylonitrile copolymer (CTBN) to a normally brittle epoxy resin significantly improved the crack resistance and impact strength without a reduction in other thermal and mechanical properties. This enhancement in crack resistance and impact strength is brought about by the formation during cure of a predominately rubbery second phase. The size of the particles making up this second phase is usually between 0.1 to 5 $\mu$m [55]. These modified thermoset resins have found wide application in structural film adhesives for metal–metal bonding in aircraft, in paste adhesives for automotive and industrial application, in electronic encapsulation, in epoxy solvent and powder coating, and in advanced aircraft and aerospace composites. However, in most epoxy applications, the final properties are strongly dependent on the morphology generated during cure of these systems. The morphology is determined by a large number of variables, such as the miscibility of the epoxy and rubber prior to cure, the cure agent, the time and temperature of cure. In some cases, optimum toughness is provided with a multi-modal distribution of particle sizes.

Siebert *et al.* [56] first described the chemistry of rubber particle formation in an admixed model involving CTBN, a liquid diglycidyl ether of bisphenol A (DGEBA) epoxy resin (Epon 828, Shell Chemical Co.), and a piperidine catalyst. They proposed that the composition of the rubber particles in the dispersed phase critically depended upon the *in situ* formation of the epoxy–CTBN–epoxy adduct, which is then further chain-extended and cross-linked with additional epoxy resin. This progression provides a chemical bond between the dispersed rubber phase and the matrix resin and occurs with piperidine, a selective catalyst. Most other cure agents, however, favour either the epoxy–epoxy reaction or an epoxy–amine reaction, and the carboxyl–epoxy reaction is suppressed. Rowe *et al.* [57] demonstrated a maximum

in fracture energy in this system when the bound acrylonitrile (AN) content of the CTBN was between 12% and 18%. They also showed a general decrease in average particle size from 3 $\mu$m at 12% bound AN to 0.2 $\mu$m at 25% bound AN.

Manzione *et al.* [58, 59] studied the morphology of an Epon 828/CTBN system and used piperidine as curative. They used three different types of CTBN rubbers – CTBN(X13), CTBN(X8) and CTBN(X15), which contain 26, 16 and 10% acrylonitrile, respectively. They used 10 p.h.r. CTBN rubber and 5 p.h.r. piperidine in the formulations, and cured the samples at three different temperatures (90, 120 and 150° C). They found all samples were phase separated except the Epon 828/CTBN (X13) compound which was cured at 150° C. This finding is of interest, although the miscibility and the phase diagrams of Epon 828/CTBN systems with or without cure agents were not investigated in their study.

A selective cure agent may enhance the carboxyl–epoxy reaction and increase the interface mixing between the epoxy and the CTBN as discussed by Siebert and Riew [56]; however, we believe that good mechanical properties can also be achieved by controlling the interface mixing between the epoxy and the rubber phase through a spinodal decomposition mechanism. As mentioned before, in the initial stage of spinodal decomposition, a gradual mixing interface develops instead of a sharp interface boundary. We believe we can control the sizes of the rubber particles by properly manipulating the kinetic processes of phase separation. Therefore, we are more concerned with the mechanism of phase separation (spinodal versus nucleation and growth) than with specific types of chemical reactions promoted by selective cure agents. Our approach to the development of morphology of epoxy–CTBN systems is therefore different from the previous studies [55–59]. We will begin by constructing miscibility gaps (binodal and spinodal curves) of uncured epoxy–CTBN systems. Then we will study the effects of cure agents on the miscibility gaps of these systems. Finally, the morphology of these systems will be manipulated through the kinetic processes of the cure reactions and subsequent phase separation. This report is mainly concerned with the miscibility and phase diagrams of epoxy–CTBN systems. A later report will deal with correlating the morphology and mechanical properties of the systems.

## 4.1. Experimental details

### *4.1.1. Sample preparation*

The epoxy resin used in this study is a low molecular weight liquid diglycidyl ether of bisphenol-A (DGEBA), Epon 828, (Shell Chemical Co). The rubber modifiers employed are low molecular weight copolymers of butadiene and acrylonitrile having carboxy end groups and manufactured under the trade name Hycar CTBN (B. F. Goodrich Co.). Three different rubber systems of varying acrylonitrile content were used in this study. Chemical and physical properties and nomenclature of the rubbers are presented in Table I. Mixtures of the rubber-modified epoxy without curatives were prepared for miscibility studies using laser light scattering. The CTBN rubber content in the mixtures was varied from 2 to 40 p.h.r. (part per hundred of epoxy resin). Samples for light scattering were prepared by hand mixing Epon 828 with CTBN (X8) at 80° C under a dry nitrogen environment and then degasing.

Samples for mechanical spectra (MS) and scanning electron microscope (SEM) measurements were prepared from degased mixtures of Epon 828/CTBN (X8) or Epon 828/CTBN (X13) containing curative. Curatives used were Versamid 140 (polyamide, Henkel Co.) or Jeffamine D230 (difunctional polyoxypropyleneamine, Texaco Chemical Co.); mixing was accomplished at 70° C under a dry nitrogen environment and then degassing. Test specimens were prepared by pouring the degased mixture into a vertical Teflon mould and curing at 120° C for 4 h under a dry nitrogen environment. Mechanical spectra were measured on a Rheometric Mechanical Spectrum (RMS). Fractured samples with exposed fresh surfaces were used for SEM measurements.

### *4.1.2. Rayleigh–Brillouin laser light scattering*

The Rayleigh–Brillouin scattering apparatus includes a triple-passed piezoelectrically scanned Fabry-Perot interferometer stabilized for both mirror parallelism and plate separation by a Burleigh DAS-1 system, a single-mode laser, and photo counting equipment. The signal was stored in a multichannel analyser (1024 channels) of the DAS-1 system. A Spectra Physics model no. 20–20 argon-ion laser operating in single-mode at 488 nm was used. All spectra were recorded at 90° angle scattering geometry. The free spectral range of the interferometer was set at 46.4 GHz and the total finesse of the whole spectrometer was 50 during all measurements.

The miscibility gap (or upper consolute temperature) of the epoxy/CTBN (X13) system (26% AN content in the CTBN) is far below room temperature. The miscibility gap of the epoxy/CTBN (X31) (10% AN content in the CTBN) is above 150° C. In order to obtain

TABLE I Physical properties of CTBN

| | Hycar polymers | | |
|---|---|---|---|
| | CTBN (1300 × 13) | CTBN (1300 × 8) | CTBN (1300 × 31) |
| Acrylonitrile content (%) | 26 | 18 | 10 |
| Molecular weight, $M_n$ | 3200 | 3600 | 3800 |
| Viscosity, cP (27° C) | 570000 | 135000 | 60000 |
| Specific gravity | 0.96 | 0.948 | 0.924 |
| Solubility parameter | 9.14 | 8.77 | 8.45 |
| Functionality | 1.8 | 1.8 | 1.9 |

TABLE II Landau-placzek ratio of epon/CTBN system

| Temperature (°C) | Landan-Placzek ratio at | | | | | | |
|---|---|---|---|---|---|---|---|
| | 2 p.h.r. | 5 p.h.r. | 10 p.h.r. | 15 p.h.r. | 20 p.h.r. | 30 p.h.r. | 40 p.h.r. |
| 22 | | | | | | | |
| 30 | | | | | | | 306 |
| 35 | | | | | | 908 | 196 |
| 40 | | 2370 | | | | 252 | 148 |
| 45 | | | | | 773 | 128 | 108 |
| 50 | 1552 | 983 | 798 | 616 | 316 | 68.4 | 73.2 |
| 55 | 946 | 455 | 610 | 498 | 168 | | |
| 60 | 406 | 473 | 425 | 230.5 | 104 | 53.3 | 48 |
| 65 | | | 238.7 | 73.5 | | | |
| 70 | 84.1 | 93.3 | 47.44 | 24.3 | 48.6 | 30.1 | 33.7 |
| 80 | 19.8 | 17.4 | 29.61 | 21.4 | 24.9 | 25.6 | 28.4 |
| 90 | 11.4 | 15 | 20.74 | 15.3 | 20.7 | 23.4 | 24.8 |
| 100 | 8.1 | 13.5 | 17.03 | 14.4 | 15.9 | 18.6 | 18.3 |

a system that could be conveniently studied near room temperature, epoxy/CTBN (X8) (16% AN content in the CTBN) was selected. The Rayleigh–Brillouin scattering data of Landau–Placzek ratio and Brillouin frequency Shift for Epon 828/CTBN (X8) at various CTBN rubber contents and temperatures are listed in Tables II and III, respectively.

## 4.2. Results and discussion

### *4.2.1. Phase diagram of rubber-modified epoxy*

Typical Rayleigh–Brillouin scattering spectra for an epoxy/CTBN sample at different temperatures are shown in Fig. 3. At the high-temperature region (Fig. 3a), there are two symmetrical Brillouin peaks located at frequencies $(\nu_0 + \nu_B)$ and $(\nu_0 - \nu_B)$. $\nu_0$ is the frequency of incident light, and $\nu_B(\omega_B = 2\pi\nu_B)$ is the longitudinal hypersonic wave of the sample. The Rayleigh peak is located at frequency $\nu_0$. The longitudinal velocity, $V_L$, and modulus, $M_L$, of the hypersonic wave of the sample can be calculated from the following formulae

$$V_L = \lambda_0 \nu_B / [2n \sin(\theta/2)] \quad (31)$$

$$M_L \approx \varrho V_L^2 \quad (32)$$

where $\lambda_0$ is the wavelength of the incident light wave, $\theta$ is the scattering angle, $n$ ($\approx 1.57$) and $\varrho$ ($\approx 1.18$) are the refractive index and density of the sample, respectively. Fig. 3a shows that the sample is in a homogeneous single phase, because a distinct and symmetrical Brillouin doublet appears in the scattering spectrum.

As temperature is decreased, an asymmetric Brillouin doublet forms as shown in Fig. 3b. This spectrum shows that the Stokes Brillouin line, at $(\nu_0 - \nu_B)$, has greater scattering intensity than the anti-Stokes Brillouin line, at $(\nu_0 + \nu_B)$. This spectrum indicates that the sample is near or on the binodal curve (phase-separation temperature). This experiment enabled us to identify the phase-separation temperature, even though the sample is still optically transparent by visual observation. The particle sizes or the domains of the sample are believed to be smaller than the incident light wavelengths. This finding is of interest and importance, because it demonstrates that Rayleigh–Brillouin scattering (RBS) is a sensitive method for studying the miscibility and phase diagrams of multiphase systems. In the RBS experiment, we defined the binodal point for each composition as the temperature where the difference of scattering intensity between Stokes Brillouin and anti-Stokes Brillouin component is about 20% (Fig. 3b). Figs 3c and d show the Brillouin spectra of fully phase-separated samples.

More than three decades ago, Debye [60, 61] and Debye Bueche [62] predicted that the angular asymmetry of the strong scattered intensity in the forward direction can be observed in the vicinity of the critical point of liquid mixtures, or in inhomogeneous systems when the particle sizes (or domain structures) are

TABLE III Brillouin frequency shift of Epon/CTBN system

| Temperature (°C) | Brillouin frequency shift ($GH_z$)at | | | | | | |
|---|---|---|---|---|---|---|---|
| | 2 p.h.r. | 5 p.h.r. | 10 p.h.r | 15 p.h.r | 20 p.h.r | 30 p.h.r. | 40 p.h.r. |
| 22 | | | | | | 10.03 | 10.09 |
| 30 | | | | | | 9.6 | 9.65 |
| 35 | | | | | | 9.44 | 9.34 |
| 40 | | 9.91 | | | 9.42 | 9.29 | 9.28 |
| 45 | | | | | 9.18 | | |
| 50 | 8.95 | 8.94 | 8.86 | 8.92 | 9.1 | 8.78 | 8.8 |
| 55 | 8.92 | 8.86 | 8.79 | 8.71 | 8.65 | | |
| 60 | 8.71 | 8.59 | 8.42 | 8.39 | 8.55 | 8.51 | 8.27 |
| 65 | | | 8.19 | | | | |
| 70 | 8.26 | 8.09 | 8.13 | 8.18 | 8.04 | 8.02 | 7.81 |
| 80 | 7.69 | 7.69 | 7.65 | 7.61 | 7.64 | 7.63 | 7.56 |
| 90 | 7.55 | 7.18 | 7.17 | 7.12 | 7.09 | 7.24 | 7.03 |
| 100 | 6.92 | 6.96 | 6.73 | 6.96 | 6.79 | 6.69 | 6.68 |

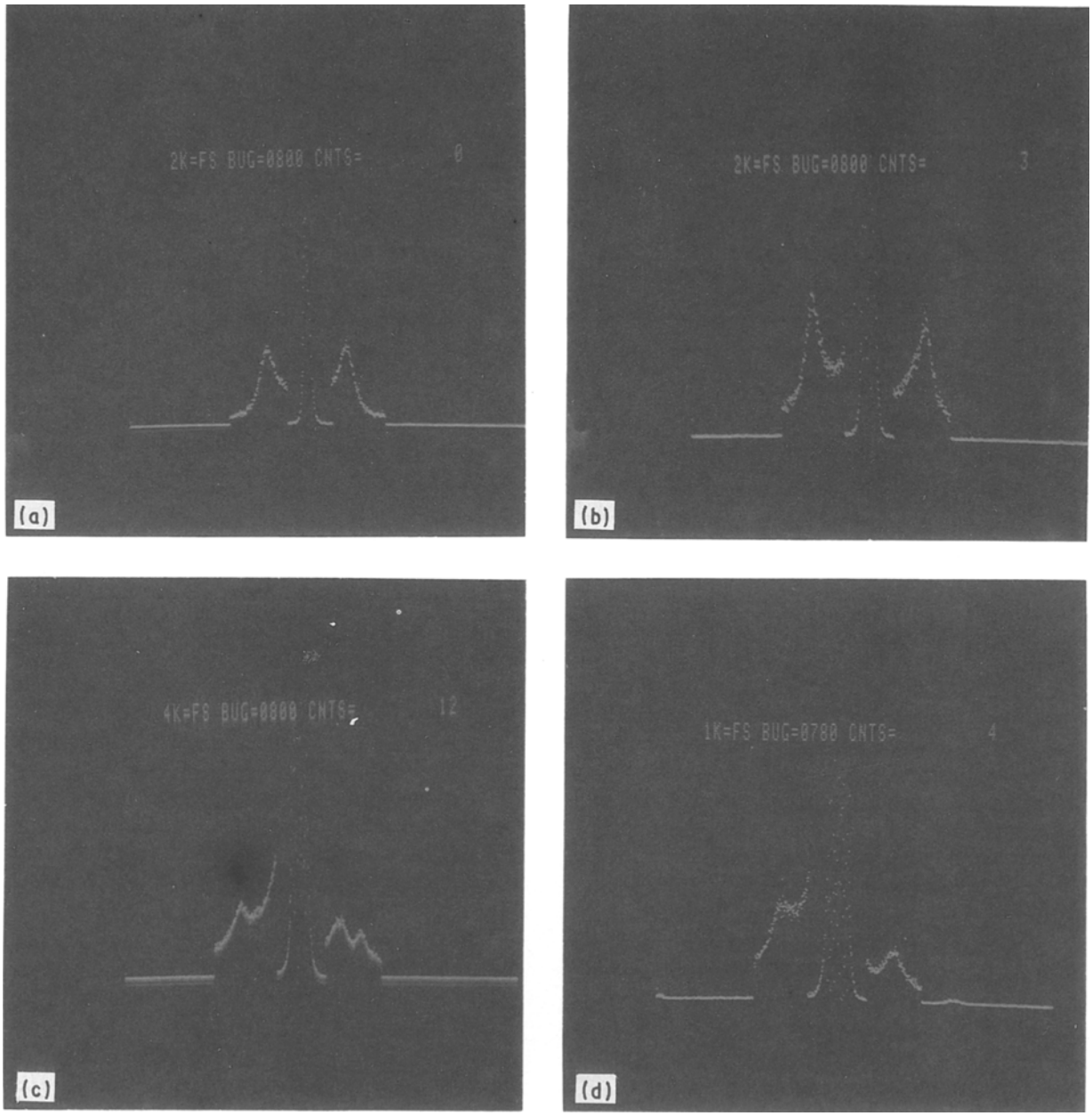


*Figure 3* Rayleigh–Brillouin spectra of epoxy 828/CTBN (X8) system with 30 p.h.r. at (a) 100° C, (b) 35° C, (c) 22° C, (d) 50° C.

larger than one-tenth of the incident light wavelength ($\approx 0.1\lambda_0$). Later Debye *et al.* [63] indeed found that a sharp increase in asymmetric scattering intensity due to incipient precipitation at the phase-separation temperature, $T_p$, which is about 1° C higher than the critical temperature (consolute temperature), $T_c$, in polystyrene/cyclohexane system. Our findings in the Rayleigh–Brillouin spectra are consistent with the prediction of the Debye theory, i.e. at the phase-separation temperature, the phenomenon of asymmetric scattering occurs. The advantage of Rayleigh–Brillouin scattering over ordinary Rayleigh scattering is that the Brillouin component is not sensitive to the impurities or inclusions of the sample (the Rayleigh component is).

The scattering spectra in Figs 3c and d were taken at the temperatures below the phase-separation temperature. At this temperature, the sample is fully phase separated and becomes opaque. The asymmetry of the two Brillouin components becomes very pronounced. Therefore, the binodal curves of the multicomponent polymer systems can be constructed by the Rayleigh–Brillouin scattering experiments, the point in the binodal curve, as shown in Fig. 4, is at the temperature where it starts to show an asymmetry of the Brillouin doublet (Fig. 3b) in each concentration of the mixtures.

Using Rayleigh–Brillouin scattering spectra to construct a spinodal curve has been discussed by Hsich *et al.* [36] and been mentioned above. As shown in Equation 30, one can easily calculate the first two terms and subtract them from the experimentally determined Landau–Placzek ratio, $R_{LP}$. Then the remaining $R_{LP}$ is expressed as the third term in Equation 30 which represents the contribution from the concentration fluctuations. As the temperature approaches the spinodal decomposition, $T_S$, the third (remaining) term, $R_{LP}(c)$, of the Landau–Placzek ratio drastically increases in accordance with the characteristics of $(T - T_S)^{-1}$. Therefore, from a

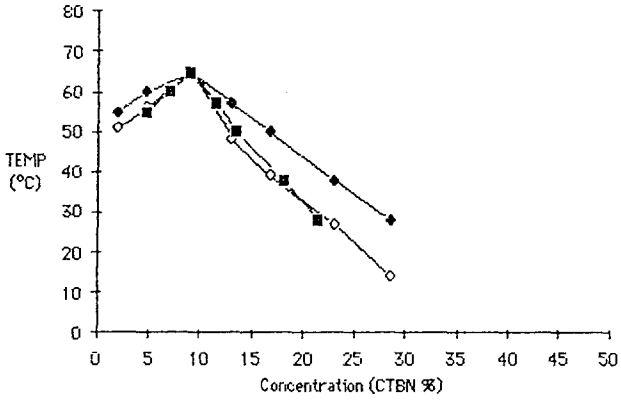


*Figure 4* Phase diagram of epoxy/CTBN. (◆) Binodal (RBS), (◇) spinodal (RBS) (■) spinodal (C–H model).

super-critical study of Rayleigh–Brillouin spectra at various temperatures, one can obtain $T_S$ of the spinodal curve by extrapolating to zero value of $1/R_{LP}(c)$ in a plot of $1/R_{LP}(c)$ against $T$.

One should keep in mind that to do an accurate calculation of $T_S$, one needs the physical properties in the first two terms of Equation 30 to calculate $R_{LP}$ from the contribution of the density fluctuations. One also needs to purify the samples to eliminate the contributions from impurities or inclusions in the Rayleigh component. However, from a practical application point of view, one can roughly estimate the spinodal curve of these polymer systems without purifying the samples or measuring all of the properties for the $R_{LP}$ calculations. To do this, Equation 30 can be simplified to

$$R_{LP} = AT + [M(\omega_B) - M_0]/M_0 + BM(\omega_B)/(T - T_S) \quad (33)$$

where $A$ and $B$ are assumed to be constants, and $M(\omega_B)$ and $M_0$ are the longitudinal moduli at the Brillouin frequency and zero frequency, respectively. The second term in Equation 33 is easily calculated. In nonrelaxational liquids, it equals zero, because the modulus is frequency independent. One can assume that $M_0 = a - bT$ [64], where $a$ and $b$ are constants. From the shift of the Brillouin frequency and Equations 31 and 32, the second term in Equation 33 can be calculated. After calculation of the second term, one can use the least squares fit to obtain the parameters of $A$, $B$, and $T_S$ in Equation 33.

The spinodal curve of Epon 828/CTBN (X8) system was constructed using this method and is shown in Fig. 4. The temperature range utilized for each composition was 100° C to the phase-separation temperature (the binodal curve). In this temperature range, the dispersion of the acoustic velocity of the epoxy system is very small, except during the cure stage. The experimental data are listed in Table II. Cook and Hilliard [65] developed a semi-empirical equation for calculating the spinodal curve by using the binodal curve. The Cook–Hilliard model is written as

$$C_s - C_c \approx (C_e - C_c)[1 - 0.422(T/T_c)] \quad (34)$$

where $C_e$, $C_s$ and $C_c$ are the concentration at equilibrium, spinodal and critical composition, respectively. The results of the calculations from Equation 34 of the Cook–Hilliard model are also plotted in Fig. 4. There is a good agreement between the Cook–Hilliard model and the current model of RBS.

### 4.2.2. Morphology and mechanical spectra of rubber-modified epoxy

As discussed above, there are two different methods for controlling morphology of multiphase systems, depending on whether cure reactions occur during material processing. In the absence of cure, the morphology can be controlled by a temperature-jump (or vaporizing the solvent) from an equilibrium and single-phase state (stable region) into a metastable, an unstable, or even another stable region. Then the formation of morphological structure will occur according to the mechanisms of phase separation as discussed above. When cure reactions predominate, the control of morphology requires the programming of cure conditions in which the system begins with a homogeneous single phase before cure reactions begin. The morphology of the system can be controlled in a homogeneously single-phase or in a heterogeneously separated phase by locking-in the morphological structure via cross-linking reactions during various stages of phase separation. Once cure reactions start, the molecular weight of the polymer system increases, the immiscibility zone is expanded and phase separation can occur. By properly manipulating the kinetics of cure and phase separation, desirable material properties can be obtained.

As mentioned earlier, the upper critical temperature is about 65° C for Epon/CTBN (X8), and is far below room temperature for Epon/CTBN (X13). However, during cure, the critical temperature (or phase-separation temperature) of these two systems will increase. Phase separation can occur even for samples that are cured at a temperature higher than the critical temperature. In this study, our purpose is to demonstrate the concept of controlling morphology via kinetics of phase separation and chemorheology regardless of curative type. The concept of locked-in morphology control is to manipulate the kinetics of phase separation by use of chemorheology during cure reactions. Two curatives were selected in this study. Versamid has a high viscosity and short gel time. This curative is believed to provide chemorheological behaviour which will reduce the kinetic ratio of phase separation by allowing morphology lock-in at the initial stage of phase separation. On the other hand, Jeffamine D230 promotes a rapid kinetic rate of phase separation.

Figs 5 to 7 illustrate the mechanical spectra of Epon/CTBN (X8). The data were measured from −80 to 120° C at a frequency of 10 rad $sec^{-1}$ and 0.3% strain. Fig. 5 represents a sample of Epon/CTBN (X8)/Jeffamine D230 having a weight ratio 100 : 40 : 32, respectively. Figs 6 and 7 describe Epon/CTBN (X8)/Versamid samples having weight ratios 100 : 40 : 50 and 100 : 10 : 50, respectively. These samples were cured at 120° C for 4 h. The glass-transition temperatures for both the rubber-rich and epoxy-rich phases, and dynamic mechanical properties at room

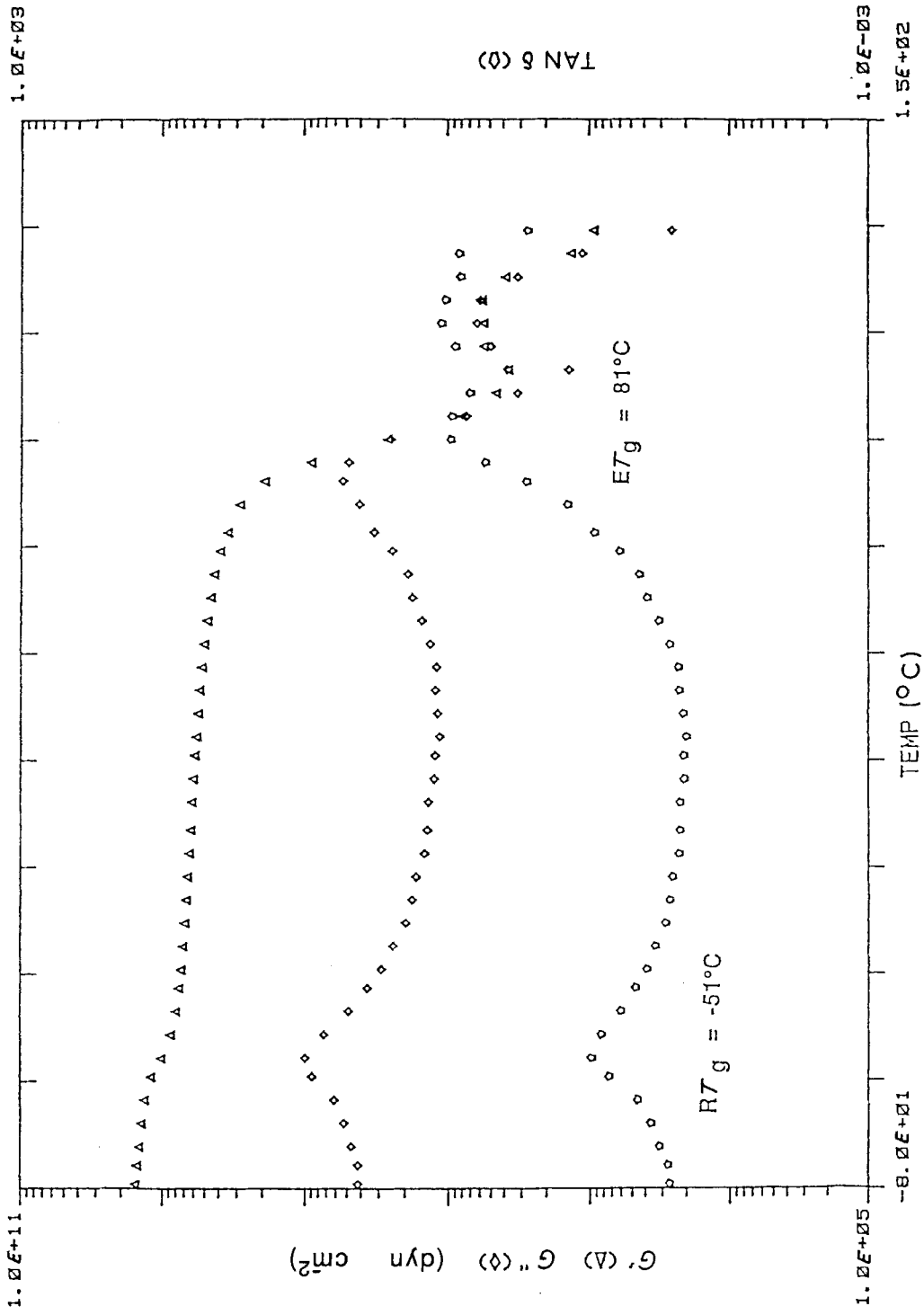


*Figure 5* Mechanical spectrum of Epon/CTBN (X8)/Jeffamine (100 : 40 : 32). $G' = 5.5 \times 10^9$, $\tan \delta = 0.021$.

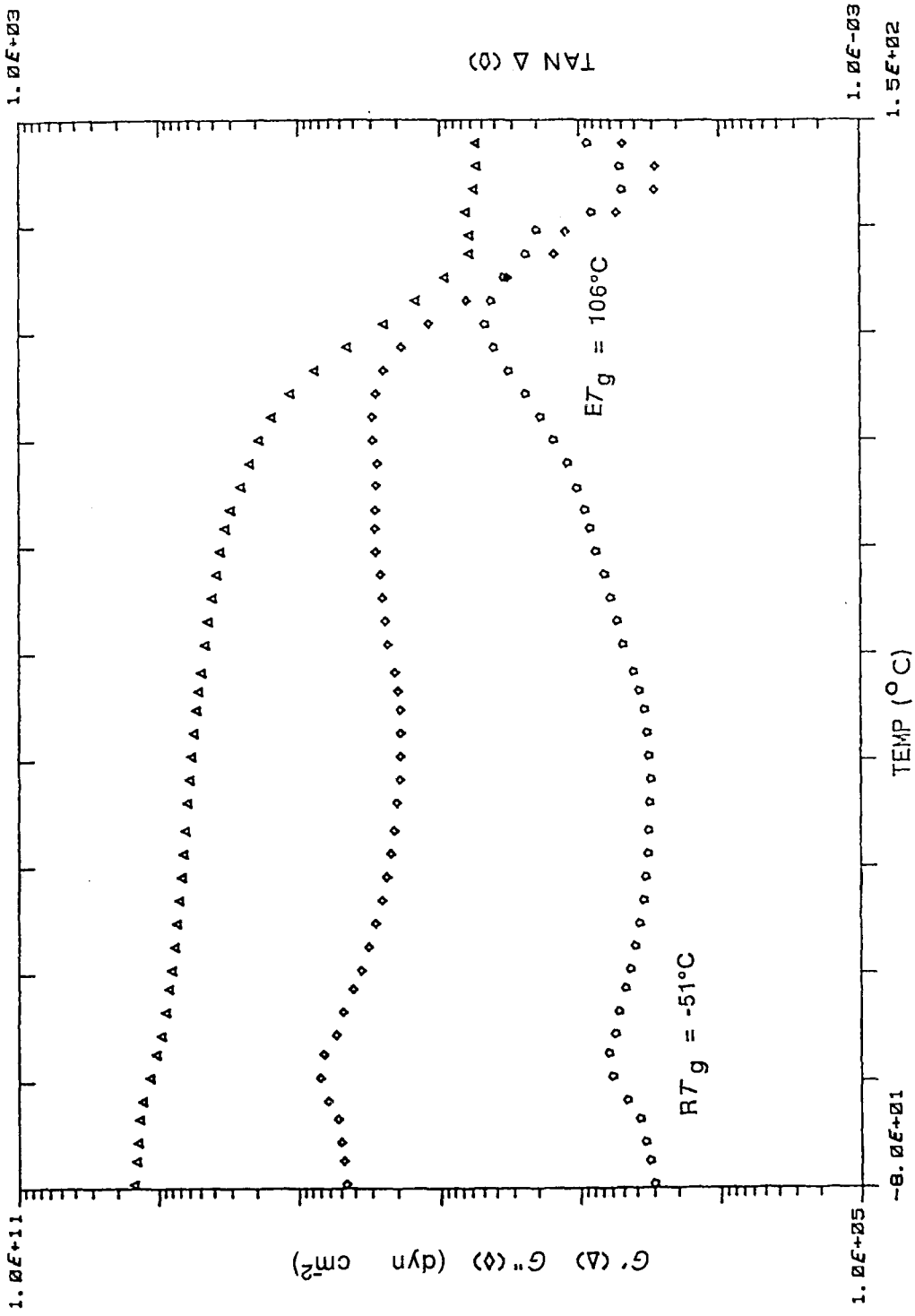


*Figure 6* Mechanical spectrum of Epon/CTBN (X8)/Versamid (100 : 40 : 50). $G' = 5.36 \times 10^9$, $\tan \delta = 0.036$.

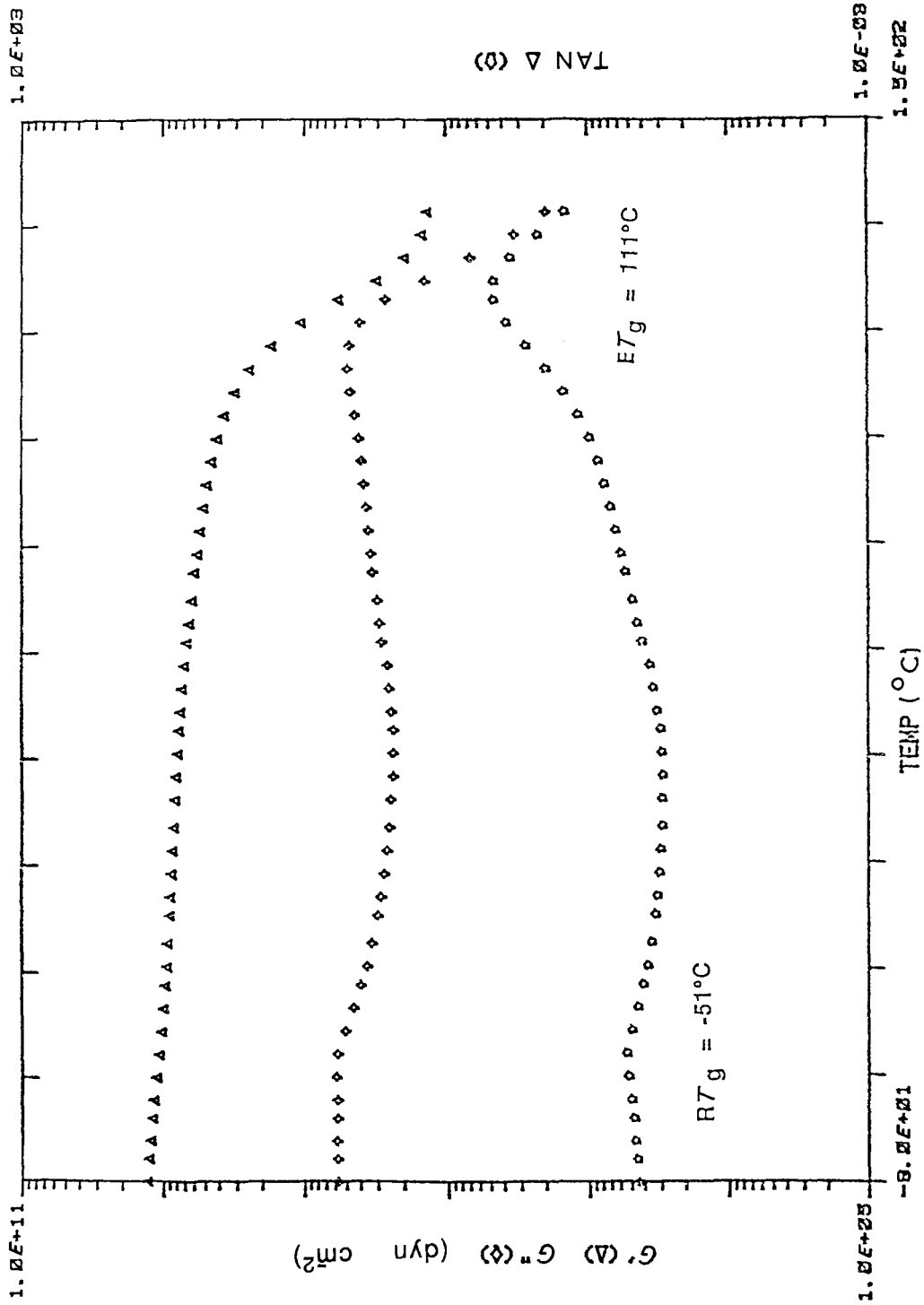


*Figure 7* Mechanical spectrum of Epon/CTBN (X8)/Versamid (100 : 10 : 50). $G' = 7.41 \times 10^9$, $\tan \delta = 0.29$.

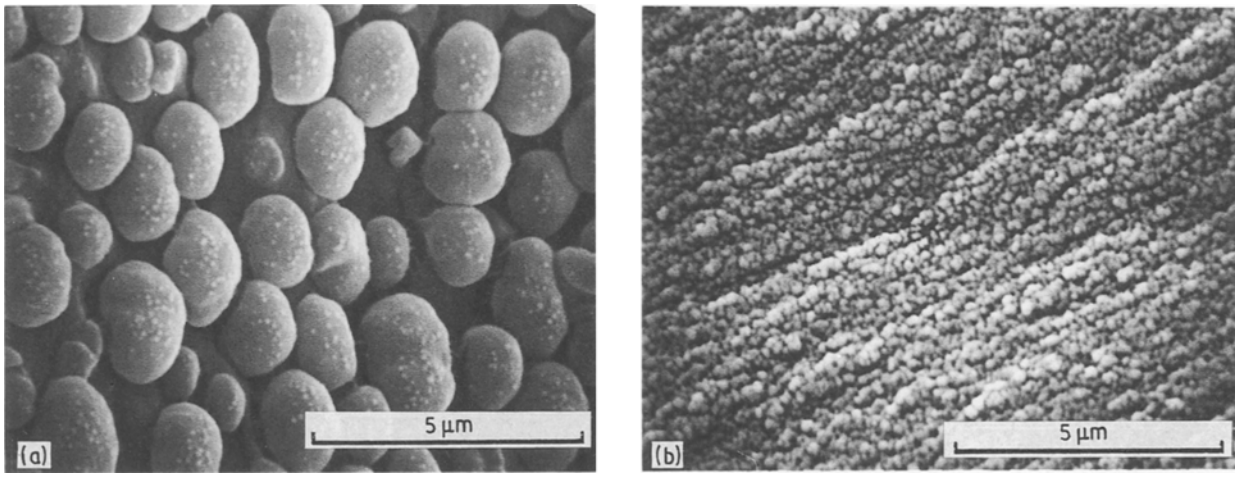


*Figure 8* Scanning electron micrographs of (a) Epon/CTBN (X8)/Jeffamine (100 : 40 : 32), (b) Epon/CTBN (X8)/Versamid (100 : 40 : 50).

temperature (22° C) are listed in Table IV . As shown in Fig. 5 and Table IV, the glass transition temperature, $T_g$ (which is defined as the temperature at the peak value of tan $\delta$), of the rubber-rich phase is $-51°$ C ($RT_g = -51°$ C), and the $T_g$ of the epoxy-rich phase is 81° C ($ET_g = 81°$ C). In this sample, the damping peak (tan $\delta$) of the rubber phase is very pronounced and $ET_g$ was not affected by the content of CTBN rubber. These results show that there was extensive phase separation in this sample. As shown in Table IV, the tan $\delta$ value for this sample is small and is close to the value obtained with zero CTBN rubber content epoxy. In fact, while the storage shear modulus for neat (no CTBN content) epoxy is somewhat higher than the sample described above, the corresponding value of $T_g$ is identical ($ET_g = 81°$ C).

The data for the Versamid-cured samples are shown in Figs 6 and 7 and are also listed in Table IV. Cure conditions used for these samples were the same as those used for the sample cured with Jeffamine. Both samples have an identical $RT_g$ ($-51°$ C), but different values of $ET_g$ which is lower than that of neat epoxy. For neat epoxies, tan $\delta$ is small and almost identical for both curatives. However, when there is an intermixing between the rubber phase and epoxy phase, tan $\delta$ increases and $ET_g$ decreases as shown in the Versamid-cured samples represented in Figs 6 and 7. If full phase separation occurs, as shown in the Jeffamine-cured sample (Fig. 5), then both values of tan $\delta$ and $ET_g$ will be similar to that of zero rubber-filled epoxy.

Figs 8 and 9 are micrographs obtained by scanning electron microscopy (SEM) $\times$ 10 000. Two different CTBN rubbers were used in the samples (Fig. 8 represents CTBN (X8), and Fig. 9 represents CTBN (X13)). All samples contained 40 p.h.r. rubber. The samples in Figs 8a and 9a were cured with Jeffamine while those in Figs 8b and 9b were cured with Versamid. $RT_g$, $ET_g$, and dynamic mechanical properties at room temperature (22° C) are listed in Table IV. As shown in Figs 8a and 9a, the size of the rubber particles varies with the particular CTBN chosen. For CTBN (X8) particle size is 2 $\mu$m but for CTBN (X13) particle size is only 0.5 $\mu$m. Both samples are optically opaque. The morphology clearly shows a droplet structure with a sharp boundary interface between the rubber and epoxy phases. This result indicates that the mechanism of phase separation for developing these morphological structures is due to nucleation and growth. The reason for this is that, during cure, the molecular weight of the polymer system is increased and, consequently, the immiscibility gap increases. Eventually, the immiscibility gap of the polymer system is raised above the cure temperature. This causes the polymer system to change from a single-phase equilibrium state to a metastable state and, therefore, phase separation is initiated by nucleation and growth. Because the immiscibility gap of

TABLE IV Properties of epoxy systems

| Epoxy system | $RT_g$ (° C) | $ET_g$ (° C) | tan $\delta$ | $G'$ ($10^9$ dyn cm$^{-2}$) |
|---|---|---|---|---|
| Epon/Jeffamine (100 : 32) | none | 81 | 0.024 | 11.3 |
| Epon/CTBN (X 8)/Jeffamine (100 : 40 : 32) | −51 | 81 | 0.021 | 5.54 |
| Epon/CTBN (X 13)/Jeffamine (100 : 40 : 32) | −32 | 81 | 0.034 | 6.11 |
| Epon/Versamid (100 : 50) | none | 121 | 0.023 | 8.29 |
| Epon/CTBN (X 8)/Versamid (100 : 10 : 50) | −51 | 111 | 0.029 | 7.41 |
| Epon/CTBN (X 8)/Versamid (100 : 40 : 50) | −51 | 106 | 0.036 | 5.36 |
| Epon/CTBN (X 13)/Versamid (100 : 40 : 50) | −32 | 101 | 0.045 | 5.02 |

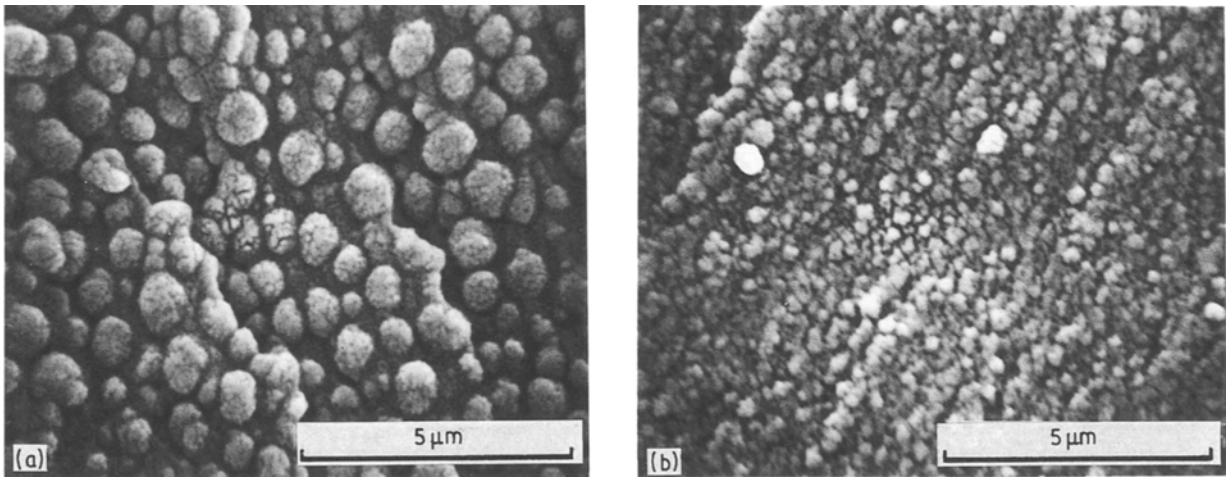


*Figure 9* Scanning electron micrographs of (a) Epon/CTBN (X13)/Jeffamine (100 : 40 : 32), (b) Epon/CTBN (X13)/Versamid (100 : 40 : 50).

Epon/CTBN (X8) is higher than that for Epon/CTBN (X13), we would expect that phase separation in Epon/CTBN (X8) would occur earlier than that in Epon/CTBN (X13) under similar cure conditions. Thus, the particle size of the rubber phase in Epon/CTBN (X8) should be larger than that in Epon/CTBN (X13). This in fact is shown in Figs 8a and 9a.

When Versamid was used to replace Jeffamine as curative, the morphological structure was drastically different as shown in Figs 8b and 9b. The chemorheological behaviour of Versamid in rubber-modified epoxy systems tends to retard the kinetics of phase separation. Nevertheless, the immiscibility gap is raised during cure, in a manner similar to the Jeffamine cured samples. Eventually, the polymer system changes from a single-phase equilibrium state to a metastable state. Initially phase separation occurs by nucleation and growth, but the retarded kinetics results in another change from the metastable state to an unstable state as molecular weight continues to increase during cure. As pointed out earlier, the kinetics of phase separation when governed by spinodal decomposition are very fast. Phase separation occurs continuously and spontaneously. Thus we found with the Versamid curative, the morphological behaviour of the samples were dominated by spinodal decomposition, as shown in Figs 8b and 9b.

Recalling Equation 19, during the initial stages of spinodal decomposition, the particle size of the rubber particle is inversely proportional to the square root of the difference between the cure temperature, $T$, and spinodal temperature, $T_s$ (i.e. $|T - T_s|^{-0.5}$). The spinodal curve ($T_s$) of Epon/CTBN (X8) is higher than that of Epon/CTBN (X13), and cure reactions will elevate the spinodal curves above the cure temperature. Once this occurs, the value of $|T - T_s|$ for Epon/CTBN (X8) is greater than $|T - T_s|$ for Epon/CTBN (X13). Consequently, the particle size of the rubber phase in Epon/CTBN (X8) should be smaller than that of Epon/CTBN (X13). This is illustrated in Figs 8b and 9b. The particle sizes of rubber shown in Figs 8b and 9b are 0.2 and 0.3 $\mu$m, respectively. These particle sizes are smaller than the wavelength of visible light and the samples are nearly transparent.

## 5. Conclusions

We have demonstrated that Rayleigh–Brillouin scattering is an effective method for studying the miscibility of multiphase systems. This method allows us to construct phase diagrams composed of both binodal and spinodal curves. We also demonstrated that the morphology of polymer alloys can be controlled by simultaneously manipulating the kinetics of phase separation and chemorheology of these alloys. We have found that the particle size of the rubber reinforcement in epoxies is effected by the mechanisms of phase separation. Phase separation by nucleation and growth gives large rubber particles than corresponding phase separation by spinodal decomposition. This contrast in the morphology development is the consequence of controlling phase separation through the chemorheological behaviour. Such control over morphology is the key to the ultimate control of mechanical properties.

## Acknowledgements

The author thanks R. J. Ambrose and K. J. Abbey for helpful discussions throughout the course of this work. In addition, appreciation is extended to M. F. Throneburgh and S. B. Watson for technical assistance in sample preparation and measurements of mechanical spectra measurement.

## References

1. D. R. PAUL, in "Polymer Blends", Vol. 2, edited by D. R. Paul and S. Newman (Academic, New York, 1978) p. 35.
2. N. E. WEEKS, F. E. FARASZ, and W. J. MacKNIGHT, *J. Appl. Phys.* **48** (1977) 4068.
3. L. M. ROBESON and J. E. McGRATH, *Polym. Engng Sci.* **17** (1977) 306.
4. S. P. TING, B. J. BULKIN, E. M. PEARCE and T. K. KWEI, *J. Polym. Sci. Polym. Chem. Edn* **19** (1981) 1451.
5. N. OHNO and J. KUMANOTANI, *Polym. J.* **11** (1979) 947.
6. T. SULZBERG and R. J. COTTER, *J. Polym. Sci. Polym. Chem. Edn* **18** (1980) 2747.
7. R. E. PRUD'HOMME, *Polym. Engng Sci.* **22** (1982) 90.
8. D. ALLARD and R. E. PRUD'HOMME, *J. Appl. Polym. Sci.* **26** (1982) 559.

9. A. EISENBERG, P. SMITH and Z. L. ZHOU, *Polym. Engng Sci.* **22** (1982) 1117.
10. Z. L. ZHOU and A. EISENBERG, *J. Polym. Sci. Polym. Phys. Edn* **21** (1983) 223.
11. M. HARA and A. EISENBERG, *Macromolecules* **17** (1984) 1335.
12. A. EISENBERG and M. HARA, *Polym. Engng Sci.* **24** (1984) 1306.
13. H. S. -Y. HSICH, *J. Mater. Sci.* **14** (1979) 2581.
14. F. M. ERNSBERGER, *Glass Ind.* **47** (1966) 422.
15. L. S. ZBORZHIL, S. AINBINDERS, V. I. BETEKHPIN, A. I. SLUTSKER, K. ALKSNE, A. I. PETROV and A. DZENIS, *Polym. Mech.* (Russian Original) **7** (1971) 817.
16. J. N. SULTAN and F. J. McGARRY, *Polym. Engng Sci.* **13** (1973) 29.
17. S. KUNZ-DOUGLASS, P. W. R. BEAUMONT and M. F. ASHBY, *J. Mater. Sci.* **15** (1980) 1109.
18. W. D. BASCOM, R. Y. TING, R. J. MOULTON, C. K. RIEW and A. R. SIEBERT, *ibid.* **16** (1981) 2657.
19. I. PRIGOGINE and R. DEFAY, "Chemical Thermodynamics", translated by D. H. Everett (Wiley, New York, 1972) Chs 16 and 18.
20. S. KRAUSE, in "Polymer Blends", Vol. 1, edited by D. R. Paul and S. Newman (Academic, New York, 1978), Ch. 1.
21. T. K. KWEI and T. T. WANG, *ibid.* Ch. 4.
22. D. TURNBULL, in "Solid State Physics: Advances in Research and Applications", Vol. 3, edited by F. Seitz and D. Turnbull, eds. (Academic, New York, 1956) p. 225.
23. I. M. LIFSHITZ and V. V. SLYOZOV, *J. Phys. Chem. Solids* **19** (1961) 35.
24. C. WAGER, *Z. Elektrochem.* **65** (1961) 581.
25. J. ZARZYCKI and F. NAUDIN, *Phys. Chem. Glasses* **8** (1967) 11.
26. J. W. CHAN and J. E. HILLIARD, *J. Chem. Phys.* **28** (1958) 258.
27. M. HILLERT, *Acta Metall.* **9** (1961) 525.
28. J. W. CAHN, *ibid.* **9** (1961) 795.
29. *Idem, J. Chem. Phys.* **42** (1965) 93.
30. J. W. CAHN and R. J. CHARLES, *Phys. Chem. Glasses* **6** (1965) 181.
31. J. W. CAHN, *Trans. Met. Soc. AIME* **242** (1968) 166.
32. K. B. RUNDMAN and J. E. HILLIARD, *Acta Metall.* **15** (1967) 1025.
33. H. E. COOK, *ibid.* **18** (1970) 297.
34. J. ZARZYCKI and F. NAUDIN, *J. Non-cryst. Solids* **1** (1969) 215.
35. W. HALLER, *J. Chem. Phys.* **42** (1965) 686.
36. H. S. -Y. HSICH, R. W. GAMMON, P. B. MACEDO and C. J. MONTROSE, *ibid.* **56** (1972) 1663.
37. H. S. -Y. HSICH, *J. Mater. Sci.* **13** (1978) 2560.
38. A. EINSTEIN, *Ann. Physik* **33** (1910) 1275.
39. L. D. LANDAU and E. M. LIFSHITZ, "Fluid Mechanics" (Academic, Reading, Massachusetts, 1959) Ch. 17.
40. L. P. KADANOFF, W. GOTZE, D. HAMBLEN, R. HECHT, E. A. S. LEWIS, V. V. PALCIQUSKAS, M. RAYL and J. SWIFT, *Rev. Mod. Phys.* **39** (1967) 395.
41. L. S. ORNSTEIN and F. ZERNIKE, *Phys. Z.* **19** (1918) 134.
42. *Idem, ibid.* **27** (1926) 761.
43. H. S. -Y. HSICH, Lord Report, CR-CD-12-87; H. S. -Y. Hsich, IR-9-87.
44. P. A. EGELSTAFF, "An Introduction to the Liquid State" (Academic, London, New York, 1967) Chs 10–12.
45. R. O. DAVIES and G. O. JONES, *Adv. Phys.* **2** (1953) 370.
46. A. J. STAVERMAN, *Rheol. Acta* **5** (1966) 283.
47. H. S. -Y. HSICH, *Amer. Ceram. Soc.* **60** (1977) 485.
48. *Idem, J. Mater. Sci.* **13** (1978) 750.
49. *Idem, ibid.* **15** (1980) 1194.
50. *Idem, J. Appl. Polym. Sci.* **27** (1982) 3265.
51. H. S. -Y. HSICH, R. M. ZURN and R. J. AMBROSE, in "Chemorheology of Thermosetting Polymers", edited by C. A. May, ACS Symposium Series no. 227 (American Chemical Society, Kansas City, Missouri, 1983) Ch. 16.
52. H. S. -Y. HSICH, L. C. YANYO and R. J. AMBROSE, *J. Appl. Polym. Sci.* **29** (1984) 2331.
53. H. S. -Y. HSICH and R. J. AMBROSE, in "Injection and Compression Molding Fundamentals," edited by A. I. Isayev, (Marcel Dekker, New York, 1987) Ch. 5.
54. R. S. DRAKE and W. J. McCARTHY, *Rubber World* **159** (October) (1968).
55. C. K. RIEW, E. H. ROWE and A. R. SIEBERT, in "Toughness and Brittleness of Plastics", edited by R. D. Deanin and A. M. Crugnola, ACS Advances in Chemistry Series no. 154 (American Chemical Society, Atlantic City, New Jersey, 1984) Ch. 12.
56. A. R. SIEBERT and C. K. RIEW, *Org. Coat. Plast. Chem.* **31** (1971) 552.
57. E. H. ROWE, A. R. SIEBERT and R. S. DRAKE, *Mod. Plast.* **47** (1970) 110.
58. L. T. MANZIONE, J. K. GILLHAM and C. A. McPHERSON, *J. Appl. Polym. Sci.* **26** (1981) 889.
59. *Idem, ibid.* **26** (1981) 907.
60. P. DEBYE, *J. Appl. Phys.* **15** (1944) 338.
61. *Idem, J. Chem. Phys.* **31** (1959) 680.
62. P. DEBYE and A. M. BUECHE, *J. Appl. Phys.* **20** (1949) 518.
63. P. DEBYE, H. COLL and D. WOERMANN, *J. Chem. Phys.* **33** (1960) 1746.
64. T. A. LITOVITZ and C. M. DAVIS, in "Physical Acoustics", Vol. IIA, edited by W. A. Mason (Academic, London and New York, 1965) Ch. 5.
65. H. E. COOK and J. E. HILLIARD, *Trans. Met. Soc. AIME* **233** (1965) 142.

*Received 31 October 1988*
*and accepted 14 April 1989*